ASME Journal of Electronic Packaging
Online journal at:
https://asmedigitalcollection.asme.org/electronicpackaging

A Comparative Numerical Analysis of Cold Plates for Thermal Management of Chips With Hotspots

Mahdi Farahikia[1]
Division of Engineering Programs,
SUNY New Platz,
1 Hawk Drive Room,
New Paltz, NY 12561
e-mail: farahikm@newpaltz.edu

Ping-Chuan Wang
Division of Engineering Programs,
SUNY New Platz,
1 Hawk Drive Room,
New Paltz, NY 12561
e-mail: wangp@newpaltz.edu

Louis Reyes
Division of Engineering Programs,
SUNY New Platz,
1 Hawk Drive,
New Paltz, NY 12561
e-mail: reyesl9@newpaltz.edu

Matthew Krumholtz
Division of Engineering Programs,
SUNY New Platz,
1 Hawk Drive,
New Paltz, NY 12561
e-mail: krumholm1@newpaltz.edu

Thermal and hydraulic performances of seven water-cooled minichannel cold plates with different internal structures are compared using numerical analysis. Recent increasing demands for high-performance computing have led to serious challenges in the thermal management of electronic devices. In addition to dangerous on-chip temperatures, heterogeneous integration and local regions of elevated temperatures (hotspots) lead to nonuniform chip-level temperature distributions. As a result, the lifespan and reliability of electronic devices are adversely impacted. Due to the limitation of the air-cooled heat sinks, several new methods, such as liquid-cooled microchannel cold plates are developed to remedy these challenges. The objective of this work is to provide a comparative numerical study of the effectiveness of different minichannel cold plate internal structures in the thermal management of a chip with a nonuniform power map and a hotspot. Cold plate thermal resistance, on-chip temperature uniformity, and pump power were the metrics used for this comparison. For four coolant inlet flow rates within the laminar regime, it is seen that increasing the inlet flowrate enhances the thermal resistance of all cold plate designs while creating less uniformity in chip-level temperature distribution relative to the conventional straight microchannels. Concentrating pin fins on the hotspot showed a 7.2% reduction in thermal resistance, despite increasing temperature nonuniformity by about 7.6%. However, it is observed that hotspot-focused pin fins are more effective in lowering the chip's maximum temperature. Obtaining lower chip-level nonuniformity may be possible by modifying the inlet and outlet conditions of the cold plates.
[DOI: 10.1115/1.4064523]

Keywords: cold plate, thermal management of microelectronics, hotspot

1 Introduction

With the increasing demand for high-performance computing, thermal management of electronic devices has met significant challenges. The temperatures of the chips reach extremely high levels in a very short time. In addition, heterogeneous integration and multicore processors lead to regions of elevated temperatures on the chip, known as hotspots. The high and nonuniform temperatures adversely affect the reliability and lifespan of the microchips.

Microchannel cold plates, first introduced by Tuckerman and Pease in 1981, showed enhanced thermal management at the chip level by taking advantage of the convection heat transfer of liquids, like water, as the coolant [1,2]. Over the years, many researchers have sought to improve chip thermal management, such as nonuniform temperature distribution, by modifying the original straight microchannel cold plate.

Xie et al. showed that narrow and deep channels in both laminar and turbulent flow regimes lead to better thermal performance but higher pressure drop penalty than wide and shallow ones in straight minichannel cold plates [3,4].

Various wavy microchannel cold plate designs were studied numerically or experimentally by Refs. [5–9]. Enhanced heat transfer and chip-level temperature distribution were reported with increasing amplitude-to-wavelength ratio of the curved channels through numerical analysis by Ghorbani et al. [5]. Mohammed et al. demonstrated numerically that these enhancements are not sustainable beyond an optimal amplitude-to-wavelength ratio of aluminum cold plates [6].

The variable-wavelength design improved local thermal performance suitable for hotspots, especially when the wavelength of the curves on high-temperature areas was smaller [8]. It was demonstrated numerically that decreasing the wavelength or increasing the amplitude of the curves along the direction of the flow lower the thermal resistance and on-chip temperature difference [9].

The hybrid microchannel-pin fin cold plates made of silicon in which pin fins were located only on the hotspot had smaller maximum hotspot temperature, thermal resistance, and chip temperature nonuniformity compared to straight microchannels [10]. Further enhancement was achieved using stepped-pin fin microchannel hybrid cold plates in which the height of the pin fins increased along the coolant flow direction [11]. The effect of various micropin fin shapes on the thermal performance of heat sinks was experimentally investigated by Hua et al. [12].

[1]Corresponding author.

Contributed by the Electronic and Photonic Packaging Division of ASME for publication in the Journal of Electronic Packaging. Manuscript received July 30, 2023; final manuscript received January 12, 2024; published online February 7, 2024. Assoc. Editor: Sukwon Choi.

 Copyright © 2024 by ASME

The effects of variable distribution of channels and flowrate on mitigating the on-chip hotspot using straight microchannel copper cold plates were studied numerically by Hadad et al. [13]. Directing more coolant flow toward the hotspot and further increasing the on-hotspot flow concentration improved the thermal response of the cold plate despite increasing the pump power.

It is obvious that many modifications of Tuckerman and Pease's microchannel cold plate and combinations of cooling methods have been studied. However, several variations exist in the performance analysis of the cooling methods in these research works. Some examples of these variations are chip power maps (uniform and nonuniform), cold plate and coolant materials, metrics for performance analysis, and coolant inlet flow conditions. To the best of our knowledge, a response comparison of different cold plates where the only variable is the internal structure of the cold plate while the other variables (such as those mentioned above) remain constant has not been extensively studied.

The present paper aims to investigate, using finite element analysis (FEA), the thermal and hydraulic responses of various water-cooled minichannel cold plate designs for a given nonuniform chip power map, coolant inlet conditions, and cold plate and coolant materials to determine a cold plate internal structural with optimum performance. Chip-level temperatures and temperature nonuniformity, thermal resistance, pressure drop, and pumping power are compared for cold plates with seven different internal structures that can be fabricated using additive manufacturing techniques for subsequent experimental verification.

The authors understand that an in-depth comparative study would lead to virtually unlimited cold plate designs with varying dimensions and geometries of the internal structure including staggered pin fins. The scope of the current work is to provide an understanding of the effectiveness of different internal structures of a cold plate in heat dissipation and the associated hydraulic cost for a unique chip power map.

2 Problem Description

Figure 1(*a*) shows the schematic of a quarter of the base cold plate design with straight minichannels, and Fig. 1(*b*) a side view of a half model. As shown in this Figure, one inlet port is used to supply the coolant flow into the cold plate. The coolant leaves the cold plate from one outlet port. A 0.1 mm thick thermal interface material (TIM) is placed between the cold plate and the chip that is located at the bottom of the cold plate.

The schematic of the square chip with arbitrarily chosen dimensions is shown in Fig. 2. A square hotspot is located at the center of the chip. The common dimensions of the model for all the seven cold plate configurations of this study are given in Table 1. The geometry and dimensions of all the different cold plate internal structures are described later in this paper.

The arbitrarily chosen heat fluxes of the hotspot and the background are 150 W/cm^2 and 20 W/cm^2, respectively. It is seen that while the hotspot covers 16% of the chip, its heat flux is 7.5 times that of the background. The total power at the chip, given by Ansari and Kim [10]

$$\dot{q}_{CH} = \dot{q}_{HS} + \dot{q}_{BG} = q''_{HS}A_{HS} + q''_{BG}A_{BG} \tag{1}$$

is 255 W. In Eq. (1), $\dot{q}_{CH}$, $\dot{q}_{HS}$, and $\dot{q}_{BG}$ represent the power at chip, hotspot, and background, respectively. q''_{HS} and q''_{BG} are the heat fluxes at the hotspot and background, and A_{HS} and A_{BG} are the areas of the hotspot and background, respectively.

The seven cold plate internal configurations investigated in this study are shown in Fig. 3. This figure shows the top view of the quarter model of these configurations, except for the layered design for which a 3-D view is given to clarify the layered structure of the channels.

The length of the channels in all configurations (l_C) is 25 mm. The length of the oblique manifold wall (l_M) at the entry and exit of the channels is 10 mm at an angle (θ) of 30 deg. The walls of the ten (10) straight minichannels in Fig. 3(*a*) are 1 mm thick (t_{CW}), and the width of the channels (w_C) is 1 mm. These dimensions apply to the straight channels in all the other configurations shown in Fig. 3. All channels, pin fins, and channel walls in this figure are 6 mm in height (h_C), and the exterior length of the inlet/outlet ports (l_{IO}) is 3 mm.

There are two straight channels on each side of the background, while an array of 13 × 6 square pin fins cover the path of the coolant through the hotspot in Fig. 3(*b*). The width and length of these pin fins (w_{SF} and l_{SF}) are 1 mm. The spacing between the pin fins is 1 mm in both horizontal ($s_{SF,H}$) and vertical ($s_{SF,H}$) directions.

The cold plate in Fig. 3(*c*) consists of two side straight minichannels and an array of 5 × 6 square pin fins concentrated on the hotspot. The dimensions of the minichannels and pin fins are the

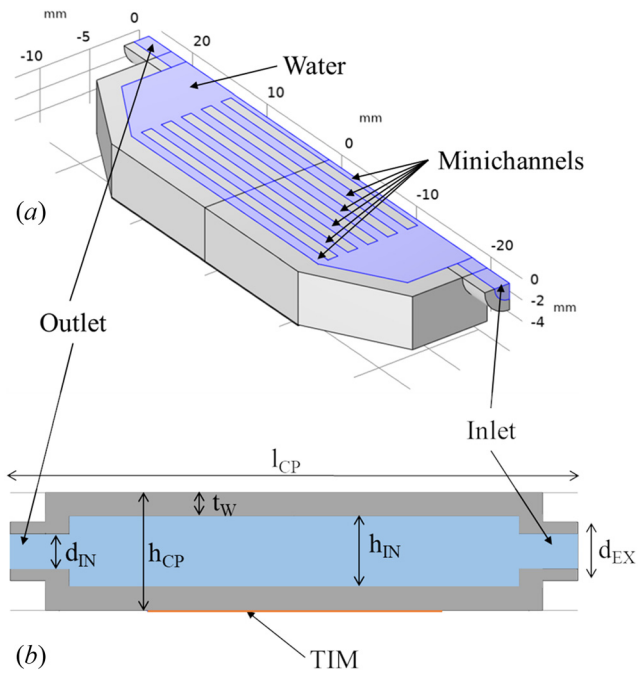

Fig. 1 (*a*) Schematic of a quarter of the base cold plate model with straight minichannels and (*b*) side view of a half model. A thin layer of TIM separates the cold plate from the chip.

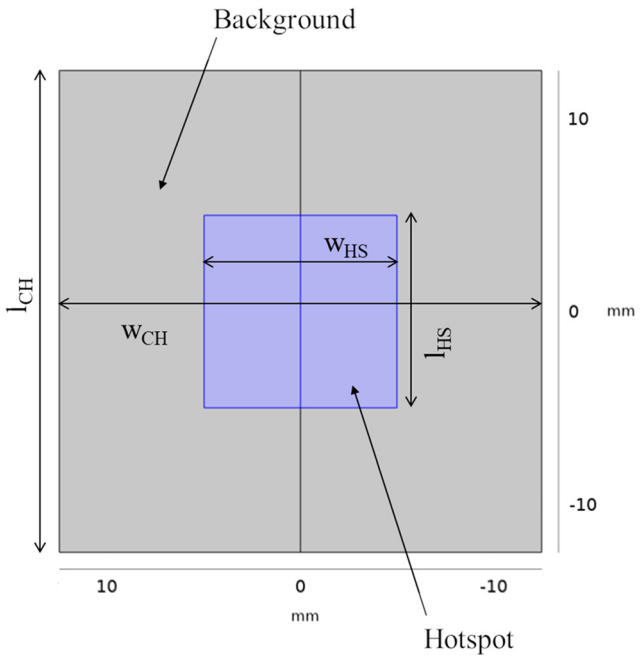

Fig. 2 A 10 mm × 10 mm hotspot is located at the center of a 25 mm × 25 mm chip

Table 1 Common dimensions for all cold plate configurations

Definition	Symbol	Value (mm)
Wall thickness	t_W	2
Inlet/outlet ext. dia.	d_{EX}	5
Inlet/outlet int. dia.	d_{IN}	3
TIM thickness	t_{TIM}	0.1
Overall cold plate height	h_{CP}	10
Cold plate internal height	h_{IN}	6
Cold plate total length	l_{CP}	48.321
Cold plate width	w_{CP}	25
Chip width	w_{CH}	25
Chip length	l_{CH}	25
Hotspot width	w_{HS}	10
Hotspot length	l_{HS}	10

same as Fig. 3(*b*). Six short minichannels of 7 mm in length (l_{SW}) are located at the entry and exit of the pin fins.

Figure 3(*d*) shows a hybrid of straight and wavy minichannels. The dimensions of the straight channels are the same as the previous designs. The wavy channels are 2.5 mm in wavelength (λ) and about 0.17 mm in amplitude (y_{WC}).

The design in Fig. 3(*e*) is similar to Fig. 3(*c*), except the pin fins are replaced by an array of 11 × 12 smaller square pin fins concentrated on the hotspot. These smaller pin fins are 0.5 mm in width (w_{PF}) and length (l_{PF}) and have 0.5 mm spacing in both horizontal ($s_{PF,H}$) and vertical ($s_{PH,V}$) directions.

In Fig. 3(*f*) a 5 × 6 array of circular pin fins of 1 mm in diameter (d_{CF}) is concentrated on the hotspot (similar to the design in Fig. 3(*c*)). The horizontal and vertical spacing ($s_{CF,H}$ and $s_{CF,V}$) of these pin fins is 1 mm, and the remainder of the cold plate geometry is the same as in Fig. 3(*c*).

A layered cold plate design is shown in Fig. 3(*g*). This design consists of three rows of eleven minichannels running along the length of the cold plate. These channels are 1 mm in width (w_C) and 1.33 mm in height (h_P). The horizontal walls are 1 mm thick (h_L).

The coolant inlet temperature (T_{in}) is 293.15 K. The four volumetric coolant inlet flow rates (q_v) in this study are 2.84, 3.55, 4.26, and 4.97 cm^3/s.

3 Numerical Analysis

3.1 Basic Assumptions. The following assumptions were made for the analyses in this work:

(1) the flow is incompressible, three-dimensional, and steady;
(2) the flow in the channels is laminar;
(3) gravity is neglected;
(4) viscous heat generation is negligible;
(5) no radiation heat transfer is present;
(6) material properties of the solid domains are constant;
(7) coolant material properties are temperature-dependent.

3.2 Governing Equations. The governing equations for a three-dimensional conduction-convection heat transfer with the above assumptions are given in the following [10,11]

The continuity equation is

$$\nabla \cdot (\rho_f \mathbf{V}) = 0 \tag{2}$$

where ρ_f is the density of the fluid and $\mathbf{V}$ is the velocity vector.

The momentum equation is

$$\mathbf{V} \cdot \nabla(\rho_f \mathbf{V}) = -\nabla P + \nabla \cdot (\mu_f \nabla \mathbf{V}) \tag{3}$$

where P is the pressure, μ_f is the absolute viscosity of the fluid.

The energy equation for the fluid is given by

$$\mathbf{V} \cdot \nabla(\rho_f C_p T_f) = \nabla \cdot (k_f \nabla T_f) \tag{4}$$

in which C_p is the specific heat capacity of the fluid at constant pressure, and k_f and T_f are the fluid conductivity and temperature, respectively.

The energy equation for the solid is

$$\nabla \cdot (k_s \nabla T_s) = 0 \tag{5}$$

where k_s and T_s represent the conductivity and temperature of the solid.

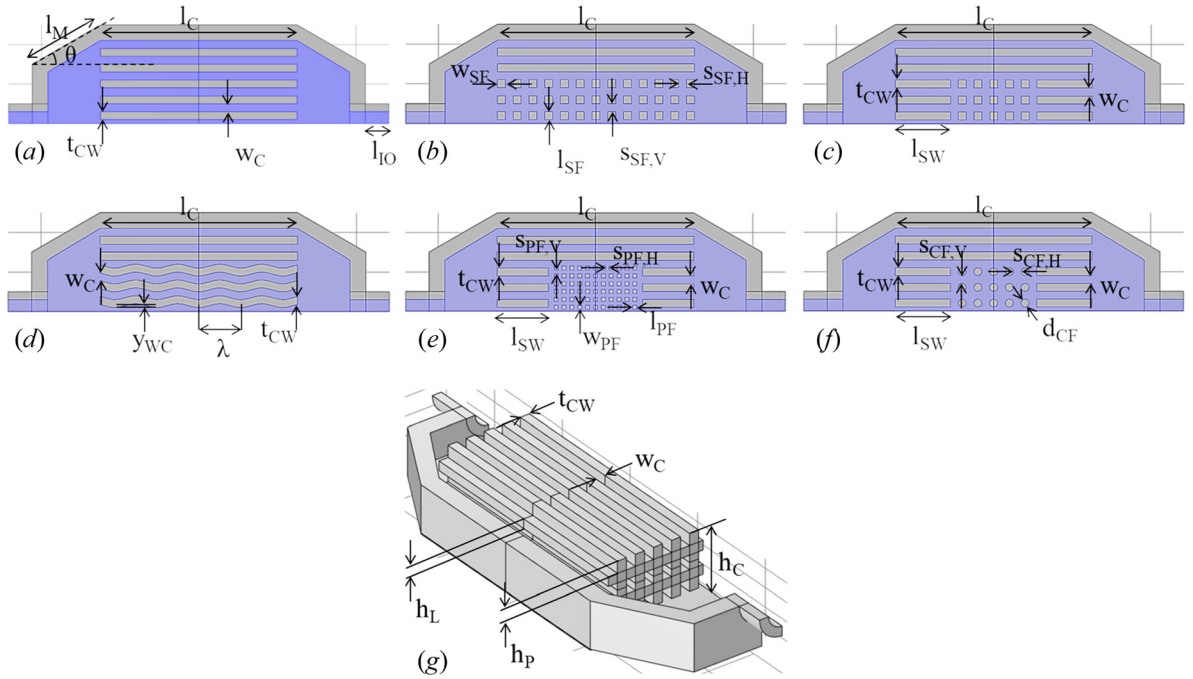

Fig. 3 Seven cold plate internal configurations: (*a*) all straight channels, (*b*) side straight channels with square pin fins on the hotspot path, (*c*) straight channels and square pin fins only on hotspot, (*d*) side straight channels and center wavy channels, (*e*) straight channels with small square pin fins on hotspot, (*f*) straight channels with circular pin fins on hotspot, and (*g*) layered straight channels

Reynolds number is given by

$$\mathrm{Re} = \frac{\rho_f u_{\mathrm{avg}} D_h}{\mu_f} \tag{6}$$

in which u_{avg} is the average fluid velocity, and D_h is the hydraulic diameter given by

$$D_h = \frac{4A_C}{P_C} \tag{7}$$

where A_C is the minichannel cross section area, P_C is the minichannel cross section perimeter. The Reynolds number in the channels and the inlet with dimensions and the highest coolant inlet velocity mentioned above range between 190 and 2100.

3.3 Boundary Conditions. Figure 4 shows the boundary conditions used in the numerical analysis of all the cold plate designs in Fig. 3. Thanks to the symmetric geometry and thermal loading of the model, half-symmetry boundary condition was applied to conserve computational resources and reduce the simulation run-time.

In Fig. 4(*a*) the coolant enters the cold plate from the "inlet velocity" surface and leaves it from the "outlet, constant pressure" surface. The four aforementioned inlet velocities were provided as normal surface velocities. Constant heat fluxes with values explained previously are applied to the hotspot and background. All the external surfaces of the cold plate, except the symmetry plane, are adiabatic. Zero-gradient boundary conditions are applied to the symmetry plane shown with the red dashed area. All the interior walls of the cold plate, except the symmetry plane, have no-slip boundary conditions, as shown in Fig. 4(*b*).

3.4 Material Properties. The numerical analysis consists of a solid domain, with one phase for the cold plate body another for TIM, and a fluid domain for the coolant. Copper was chosen as the material for the cold plate and thermal grease was used for TIM. The thermophysical properties of copper and TIM are given in Table 2.

As mentioned earlier, a temperature-dependent material model of water was used here. The density (ρ), specific heat (c_p), thermal conductivity (k), and dynamic viscosity (μ) of liquid water (273.15 K < T < 373.15 K), used in COMSOL, are as follows:

$$\rho = -950.70406 + 18.92294T - 0.06037T^2 + 0.00006T^3 \tag{8}$$

$$c_p = 12010.1471 - 80.4073T + 0.3099T^2 - (5.3817 \times 10^{-4})T^3 + (3.6254 \times 10^{-7})T^4 \tag{9}$$

$$k = -0.8691 + 0.0089T - (1.5837 \times 10^{-5})T^2 + (7.9754 \times 10^{-9})T^3 \tag{10}$$

$$\mu = 1.3799 - 0.0212T + (1.3605 \times 10^{-4})T^2 - (4.6454 \times 10^{-7})T^3 + (8.9043 \times 10^{-10})T^4 - (9.0791 \times 10^{-13})T^5 + (3.8457 \times 10^{-16})T^6 \tag{11}$$

In these equations, T is temperature in K.

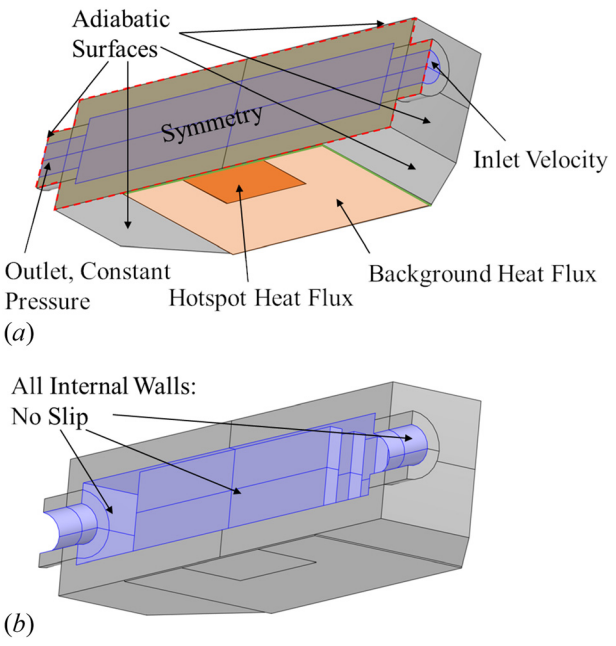

Fig. 4 Schematic of the numerical domain and boundary conditions. Half-symmetry analysis was possible due to the symmetric geometry and boundary conditions.

3.5 Numerical Method. COMSOL commercial finite element analysis (FEA) software was used to perform conjugate heat transfer analysis with laminar fluid flow. Conjugate heat transfer analysis implies that the temperatures in the fluid and solid domains are calculated simultaneously [3].

4 Mesh Sensitivity

Mesh sensitivity analysis was conducted for thermal resistance (R_{th}'') and pump power ($\dot{W}_P$) defined later in Eqs. (12) and (15), respectively. It is seen in Fig. 5 that with more than 1×10^6 elements, the deviation of results is less than 2%. Hence, the mesh quality shown by the dashed area was selected.

5 Discussion of Results

5.1 Thermal Resistance. The thermal response a cold plate is reflected by its thermal resistance, given by Hadad et al. [13]

$$R_{\mathrm{th}}'' = \frac{A_{CH}(T_{c,\max} - T_{\mathrm{in}})}{\dot{q}_{\mathrm{CH}}} \tag{12}$$

where $T_{c,\max}$ and T_{in} are the maximum chip temperature and the coolant inlet temperature, respectively, and A_{CH} is the chip area. Lower thermal resistance yields higher heat transfer rate which is desired in the thermal management of micro-electronics.

Thermal resistances of all the cold plate configurations as a function of the coolant inlet flowrate are shown in Fig. 6. The cold plate with small square pin fins on the hotspot has the lowest thermal resistance, which is about 10.13% lower than that of the straight channel. Thermal resistance of the cold plates with square pin fins covering the coolant path to the hotspot, square pin fins only on the hotspot, and layered channels (Figs. 3(*b*), 3(*c*), and 3(*g*), respectively) are similar and between 4.5% to 6.0% less than the straight channel. This could be due to increased surface area on the hotspot of the pin fins and layered channels. The curved channel and circular pin fin configurations show thermal resistances very close to that of the straight channel.

The surface area of the circular pin fins is about 21.46% smaller than the square pin fins. This can lead to less heat transfer from the hotspot, hence, higher thermal resistance.

5.2 Chip Temperature Uniformity. The ultimate objective of cooling devices is to lower the chip temperature and achieve

Table 2 Thermophysical properties of copper and TIM

	c_p(J/kg · K)	k(W/m · K)	ρ(kg/m^3)
Copper	385	400	8960
TIM	1200	3	2600

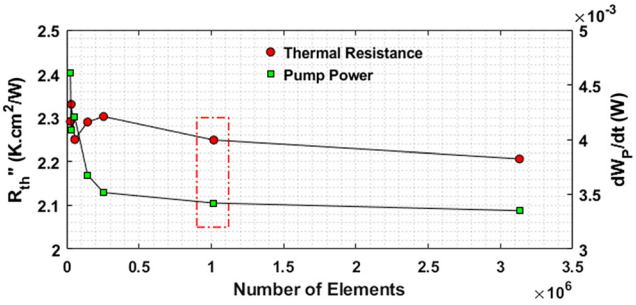

Fig. 5 Mesh sensitivity analysis

quasi-uniform temperature distribution on the chip [14,15]. Several parameters have been used by researchers including those cited in this work to examine chip temperature uniformity as an important performance metric. Here, this metric is defined by Hadad et al. [13]

$$\psi = \frac{T_{c,\max} - T_{\text{in}}}{T_{c,\min} - T_{\text{in}}} \tag{13}$$

in which $T_{c,\min}$ is the minimum chip temperature. For an ideally uniform chip-level temperature distribution, it is required that $T_{c,\max} = T_{c,\min}$, or $\psi = 1$ [13].

Normalized chip temperature uniformity as a function of coolant inlet flowrate is shown in Fig. 7. It is seen that chip temperature distribution is the least uniform for the small pin fin in comparison with the straight channel configuration despite having lower thermal resistance. While circular pin fins and curved channel configurations have similar temperature distribution to the straight channel with less than 5% difference, the "all pin fin" configuration (see Fig. 3(*b*)) has the second highest nonuniform temperature distribution with an average deviation of about 18.55%.

The normalized chip temperature uniformity of the cold plate configuration with square pin fins only on the hotspot (see Fig. 3(*c*)) is 6.51% higher than the straight channel on average while showing lower thermal resistance.

5.3 Chip Maximum and Minimum Temperatures. To understand the thermal resistance and temperature distribution observed above, the difference in maximum and minimum chip temperature with respect to the coolant inlet temperature, given by

$$\begin{aligned} \Delta T_{\max} &= T_{c,\max} - T_{\text{in}} \\ \Delta T_{\min} &= T_{c,\min} - T_{\text{in}} \end{aligned} \tag{14}$$

are studied.

The differences in maximum and minimum chip temperatures relative to the coolant inlet temperature are shown in Figs. 8(*a*) and 8(*b*), respectively. It is seen in this figure that the maximum chip

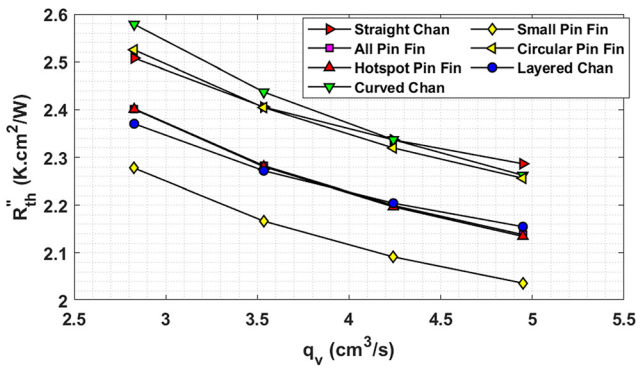

Fig. 6 Thermal Resistance of the cold plates show a decreasing trend with increasing coolant flowrate

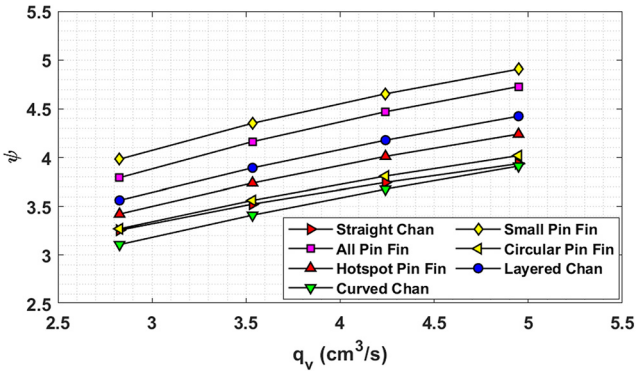

Fig. 7 Chip-level temperature distribution as a function of coolant flowrate

temperatures that are expected to be on the hotspot follow the same trend as seen for thermal resistance in Fig. 6.

The small pin fin configuration has the lowest maximum chip temperature, while the configurations with square pin fins (see Figs. 3(*b*) and 3(*c*)) and the layered channels (see Fig. 3(*g*)) have similar maximum chip temperatures. Placement of pin fins with higher surface on the hotspot, leading to enhanced heat transfer, can explain this observation.

The cold plate design with small pin fins on the hotspot also has the lowest minimum chip temperature. This can imply that this design has a better heat transfer rate on the hotspot but also overcools the background. As a result, there is a bigger difference between the maximum and minimum chip temperatures. A possible reason for this, currently under investigation, may be that some of the heat generated in the background is dissipated through the small pin fins via spreading in the cold plate base.

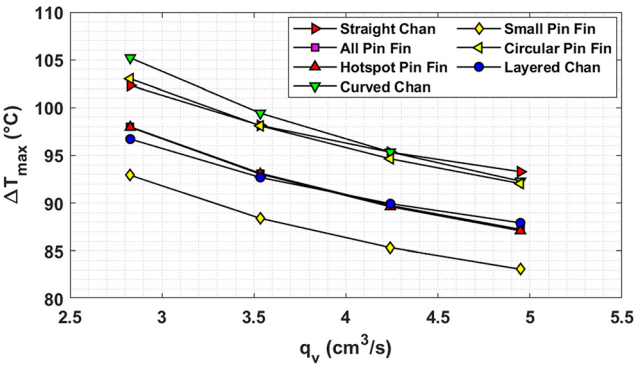

(*a*)

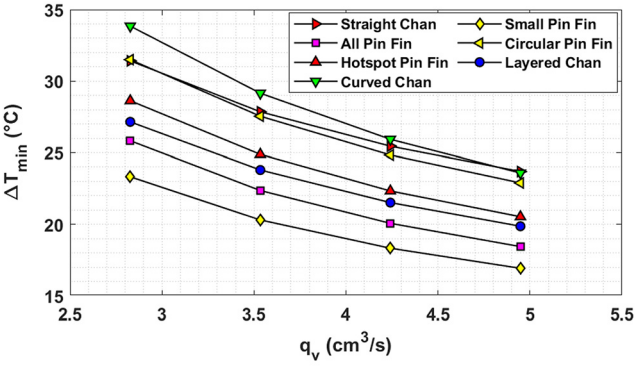

(*b*)

Fig. 8 Chip maximum and minimum temperature difference with respect to coolant inlet temperature

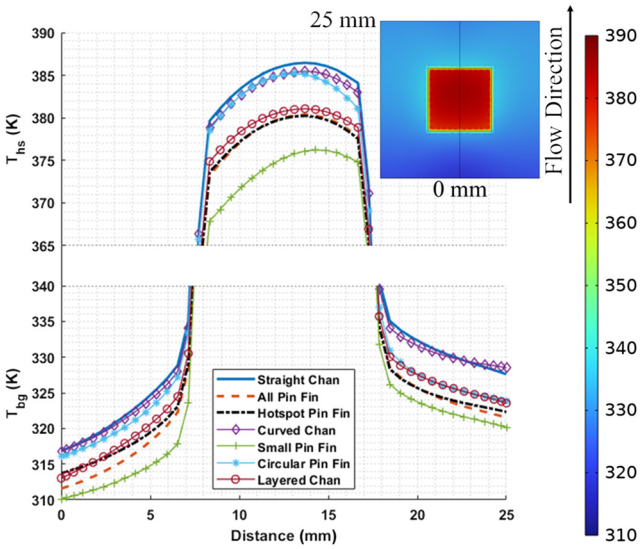

Fig. 9 Chip temperature profile along the line of the coolant flow. A typical chip-level temperature distribution is shown.

Among the designs with square pin fins (Figs. 3(*b*) and 3(*c*)) and layered channels (Fig. 3(*g*)), the one with pin fins only on the hotspot has a higher minimum chip temperature. That leads to a smaller difference between the maximum and minimum chip temperatures on the chip with this cold plate. Although the temperature distribution with this cold plate seems more nonuniform than the straight channel, curved channel, and circular pin fin configurations, it is important to note that the latter three configurations tend to undercool the hotspot. As a result, the chip temperature possibly remains dangerously high on the hotspot.

Chip-level temperature profile along the line of the coolant flow is shown in Fig. 9. The colormap in this Figure represents the typical chip-level temperature distribution for all the cold plate configurations. Figure 9 shows a significant difference between the chip temperature on the hotspot and background, demonstrating a nonuniform temperature distribution.

5.4 Pump Power. The efficiency of a cold plate can be determined by the pump power required to dissipate heat. An efficient cold plate requires less pump power to dissipate more heat from the chip [14]. Pump power is a function of pressure drop and coolant flowrate and is calculated using Eq. (15)

$$\dot{W}_P = \Delta P \cdot q_v \tag{15}$$

Figure 10 shows the pump power given by Eq. (15). This figure shows that the deviation on pump power among the seven

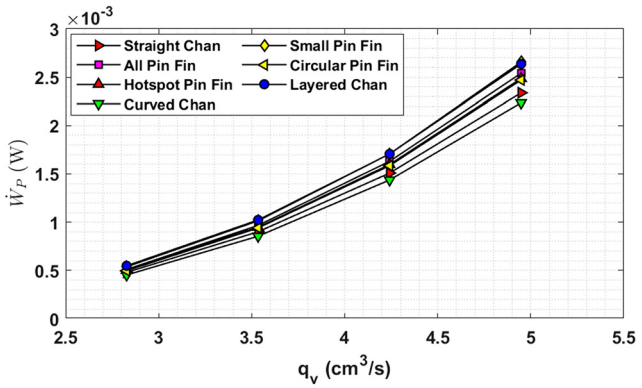

Fig. 10 Pump power as a function of coolant inlet flowrate

configurations studied in this work is bigger at higher coolant inlet flowrate. The curved channel design gives about 5% less pump power than the straight channel cold plate. In contrast, the cold plate with square pin fins on the hotspot (Fig. 3(*c*)) leads to 4.6% to 6.3% increase in pump power relative to the straight channel design.

6 Conclusion

A comparative analysis was performed for seven cold plate designs and four coolant inlet velocities using COMSOL. The only variable in this study was the internal structure of the cold plate while other parameters such as material properties, coolant inlet conditions, and chip power map were unchanged.

The presence of pin fins on the hotspot led to an enhanced heat transfer rate and a reduction in its temperature, hence, lower thermal resistance. However, smaller square pin fins concentrated on the hotspot showed an adverse effect on the on-chip temperature uniformity due to overcooling the background. Circular pin fins with a smaller surface area yielded higher thermal resistance than square pin fins.

While the on-chip temperature distribution was more nonuniform using cold plates with square pin fins relative to circular pin fins and straight channels, the latter designs resulted in lower heat transfer rates on the hotspot, undercooling it and leading to higher chip temperatures. Hence, a balance between thermal resistance and temperature distribution should be considered for a choice of a cold plate design for the thermal management of chips with hotspots.

Hydraulic response comparison of the cold plate designs showed that the gain in thermal performance comes at the cost of pressure drop penalty and increased pump power. Overall, the cold plate with 1×1 mm^2 squared pin fins on the hotspot studied in the present work showed an optimal performance considering thermal and hydraulic responses. Results of the on-going experimental characterization will be reported separately.

Acknowledgment

We wish to thank the office of Research, Scholarship, and Creative Activities at SUNY New Paltz. We also wish to thank Hudson Valley Additive Manufacturing Center at SUNY New Paltz for advice on metal 3-D printing.

Data Availability Statement

The datasets generated and supporting the findings of this article are obtainable from the corresponding author upon reasonable request.

References

[1] Tuckerman, D. B., and Pease, R. F. W., 1981, "High-Performance Heat Sinking for VLSI," IEEE Electron Device Lett., **2**(5), pp. 126–129.

[2] Phillips, R. J., 1987, "Forced-Convection, Liquid-Cooled, Microchannel Heat Sinks," Ph.D. thesis, Massachusetts Institute of Technology, Cambridge, MA.

[3] Xie, X., Tao, W., and He, Y., 2007, "Numerical Study of Turbulent Heat Transfer and Pressure Drop Characteristics in a Water-Cooled Minichannel Heat Sink," ASME J. Electron. Packag., **129**(3), pp. 247–255.

[4] Xie, X., Liu, Z., He, Y., and Tao, W., 2009, "Numerical Study of Laminar Heat Transfer and Pressure Drop Characteristics in a Water-Cooled Minichannel Heat Sink," Appl. Therm. Eng., **29**(1), pp. 64–74.

[5] Ghorbani, N., Targhi, M. Z., Heyhat, M. M., and Alihosseini, Y., 2022, "Investigation of Wavy Microchannel Ability on Electronic Devices Cooling With the Case Study of Choosing the Most Efficient Microchannel Pattern," Sci. Rep., **12**(1), pp. 5882–5902.

[6] Mohammed, H., Gunnasegaran, P., and Shuaib, N., 2011, "Numerical Simulation of Heat Transfer Enhancement in Wavy Microchannel Heat Sink," Int. Commun. Heat Mass Transfer, **38**(1), pp. 63–68.

[7] Sui, Y., Lee, P., and Teo, C., 2011, "An Experimental Study of Flow Friction and Heat Transfer in Wavy Microchannels With Rectangular Cross Section," Int. J. Therm. Sci., **50**(12), pp. 2473–2482.

[8] Sui, Y., Teo, C., Lee, P. S., Chew, Y., and Shu, C., 2010, "Fluid Flow and Heat Transfer in Wavy Microchannels," Int. J. Heat Mass Transfer, **53**(13–14), pp. 2760–2772.

[9] Lin, L., Zhao, J., Lu, G., Wang, X.-D., and Yan, W.-M., 2017, "Heat Transfer Enhancement in Microchannel Heat Sink by Wavy Channel With Changing Wavelength/Amplitude," Int. J. Therm. Sci., **118**, pp. 423–434.

[10] Ansari, D., and Kim, K.-Y., 2018, "Hotspot Thermal Management Using a Microchannel-Pinfin Hybrid Heat Sink," Int. J. Therm. Sci., **134**, pp. 27–39.
[11] Ansari, D., and Kim, K.-Y., 2019, "Hotspot Management Using a Hybrid Heat Sink With Stepped Pin-Fins," Numer. Heat Transfer, Part A: Appl., **75**(6), pp. 359–380.
[12] Hua, J., Li, G., Zhao, X., and Li, Q., 2017, "Experimental Study on Thermal Performance of Micro Pin Fin Heat Sinks With Various Shapes," Heat Mass Transfer, **53**(3), pp. 1093–1104.
[13] Hadad, Y., Radmard, V., Rangarajan, S., Farahikia, M., Refai-Ahmed, G., Chiarot, P. R., and Sammakia, B., 2021, "Minimizing the Effects of on-Chip Hotspots Using Multi-Objective Optimization of Flow Distribution in Water-Cooled Parallel Microchannel Heatsinks," ASME J. Electron. Packag., **143**(2), pp. 021007–021017.
[14] Gonzalez-Valle, C. U., Samir, S., and Ramos-Alvarado, B., 2020, "Experimental Investigation of the Cooling Performance of 3-D Printed Hybrid Water-Cooled Heat Sinks," Appl. Therm. Eng., **168**, pp. 114823–114831.
[15] Hao, X., Peng, B., Xie, G., and Chen, Y., 2016, "Efficient on-Chip Hotspot Removal Combined Solution of Thermoelectric Cooler and Mini-Channel Heat Sink," Appl. Therm. Eng., **100**, pp. 170–178.